Molecular dynamics simulations of 2D-confined water

Thorin Bristow

School of Physics and Astronomy

University of Manchester

MPhys Project

This project was performed in collaboration with Izaak Lee.

May 2021

Molecular dynamics simulations were performed on a system of water molecules confined between two graphene layers with periodic boundary conditions. The graphene layers are atomically flat, homogenous, and free of defects. The analyses described in this report build upon the work carried out in first semester, with further investigations into the structural properties of the system, and water at the interface. In particular, the orientation of the water molecules (and hence dipoles) at the interface.

Contents

1. Introduction

The structure of liquid water confined between nonpolar surfaces has been investigated using computer simulation methods for many years [1]. The development of techniques to isolate graphite layers to form graphene [2, 3] have created new opportunities for exploring the properties of water at the interface with hydrophobic surfaces. In graphene, carbon atoms are located in the nodes of a two-dimensional honeycomb lattice with covalent bonding between atoms [4]. The motivation for this project was to further a theoretical explanation for an anomalously low value of the dielectric constant of confined water reported by Fumagalli *et al.* in 2018 [5]. The researchers measured an out-of-plane dielectric constant of ~ 2 for water strongly confined between two graphene walls separated by a few angstroms, where the dielectric constant of bulk water is ~ 80 having full rotational freedom of water dipoles. Theoretical support for this phenomenon was lacking, hence the focus of this project has been on atomistic simulations of a comparable confined-water system.

An understanding of the behaviour of interfacial water is crucial for understanding many processes in biology and geochemisty, among others. The properties of confined water play an important role in many biomolecular systems including transport in intracellular environments and via ion channels [6]. The interaction between water and hydrophobic surfaces also accounts for a number of biological self-assembly processes such as membrane formation and protein folding [7,8], as well as applications for energy storage with water electrolysis [9]. The graphene surfaces are considered hydrophobic because the interactions between the surface and the water molecules is nonpolar [10].

Simulations are an effective tool that can replace experiment, or help explain previous results and provide connections with theory. In many cases, experiments are expensive, time consuming and difficult to perform. Simulation allows us to control the many parameters of the system with greater accuracy than experiment, and can give insight into the properties of materials at the atomic or molecular level. Furthermore, simulations can be used to compute numerical solutions in cases where analytical solutions are impossible. This is the case for solving the equations of motion for a system of water

molecules, where the forces acting on each individual atom can be determined, provided a suitable potential is used, and both the vector distances between atoms and the total number of atoms in the system are known [11].

We investigated the water molecule orientation at the interface, and how this depends on the density of the system. The probability distributions for the dipole orientations and hydrogen bond angles are presented. Additionally, radial pair distribution functions were obtained for hydrogen-hydrogen and oxygen-hydrogen networks, where previously only oxygen-oxygen distribution functions were presented. The distribution of the average number of hydrogen bonds per molecule is also presented. These are a continuity of the work carried out in the previous semester investigating the structural properties of water at the interface.

1.1. Outline of previous semester's work

In the previous semesters' work, the oscillatory structure of the density profile of water confined between two graphene surfaces was successfully reproduced. This was done at three densities: $1.0, 1.2$ and 1.4 g/cm^3. A bulk water system was also simulated at the same densities, to benchmark our simulation model and provide data that could be used to inform our results for the confined system. In all confined simulations, an interfacial layer of a few angstroms across is formed, which is consistent with previous studies on water at carbon-based interfaces [12, 13]. From previous work, the plots of mass density distribution, number of hydrogen bonds per molecule, and oxygen-oxygen pair distribution functions, are included in Appendix A.

We concluded that the suppressed rotational freedom of water dipoles under extreme confinement with the interfacial layering effects is crucial for explaining the anomalously low value of the dielectric constant [5].

2. Methodological approach

2.1. Simulation details

Last semester, we performed molecular dynamics simulations using LAMMPS[1] [14] for two different systems, one bulk and one confined, at three different densities. LAMMPS is an open-sourced public software for classical molecular dynamics simulation, used extensively for modelling materials at the mesoscale. Software such as LAMMPS are used to solve Newton's equations of motion for many-particle systems, and hence require interatomic potentials (force fields) to be defined in order to compute the forces. The forces on an individual atom or molecule are determined by the force field, the number of atoms or molecules in the system (denoted N), and the vector distance between each atom (denoted r_{ij}). For our simulations, we generated initial configurations of atoms using packmol [15], a program which packs molecules in a defined region of space (simulation box) and ensures that short-range repulsive forces do not cause breakdown of the simulation in the first few timesteps. The corresponding force field input files were built using fftool [16].

This semester we developed our analysis of the confined case. The number of water molecules composing the confined and bulk systems at each density are given in Table 1, with the confined system illustrated in Figure 1. The confined system parameters were $36.892682x \times 38.334000y \times 30.000000z$, with each graphene sheet consisting of 540 carbon atoms. Note that the separation between the graphene sheets (z-axis) was fixed at 3.0 nm for all simulations. Periodic boundary conditions were imposed along the x and y axes to eliminate edge effects [17]. The cutoff value was half the box length at each axis, where the $[x, y, z]$ box lengths for the confined system were [18.446341×2, 19.167000×2, 100] in angstroms. The value of 100Å in z is used so that the periodic boundary conditions are not applied in the z-axis. A diagrammatical representation of periodic boundaries is shown in Figure 2.

The water molecules were modelled using the SPC/E pair potential [18], and long-

[1]Large-scale Atomic/Molecular Massively Parallel Simulator

range electrostatic interactions were modelled using Ewald summation [19]. In this model, the oxygen atoms also interact with the graphene walls via a Lennard-Jones potential [20]. The simulations were carried out at ambient temperature (298K), using the NVT (canonical) ensemble which allowed the temperature to be controlled using a thermostat. The hydrogen-oxygen bond length was held fixed at 1Å, and the hydrogen-oxygen-hydrogen bond angle at 109.5 degrees. For two atoms to be considered hydrogen bonded, the oxygen-oxygen distance must be less than 3.5Å and the oxygen-hydrogen distance between donor and acceptor atoms must be less than 2.4Å.

Table 1: The number of water molecules, N_w, in each of the simulations.

Density (g/cm^3)	N_w^{Confined}	N_w^{Bulk}
1.0	1245	3900
1.2	1500	4680
1.4	1751	5460

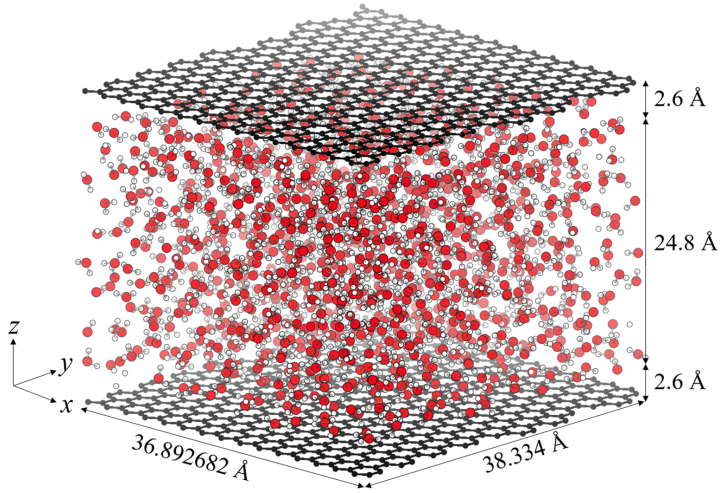

Figure 1: The confined system configuration studied. This visualisation was rendered using VMD [21].

An important aspect of running MD simulations is that before data can be collected and results analysed, the system must be prepared via phases of equilibration. This is

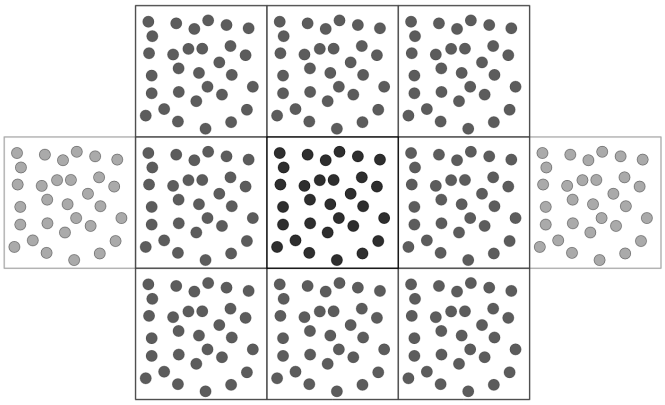

Figure 2: A diagrammatical representation of periodic boundary conditions in two dimensions [22].

to achieve stability before the production run is carried out. During the equilibration phase, Newton's equations of motion are solved for the system of N particles until the properties of the system no longer change with time [11]. Furthermore, this phase allows the energy of the system to converge and achieve thermodynamic equilibrium. This is essential as the computed averages over the production run only have physical sense at thermodynamic equilibrium. After equilibration, the production run is carried out, from which time averages can be computed and structural properties calculated (such as radial pair distribution functions for molecular liquids). The simulation runtimes and timesteps are outlined in Table 2. As can be seen, the system was equilibrated for 2 nanoseconds. This was followed by a production run of 5 nanoseconds during which snapshots were taken every picosecond.

Table 2: Timesteps and runtimes for each stage of simulation.

Stage	Timestep	Total steps	Total runtime
Pre-equilibration	0.5 fs	1000	0.5 ps
Equilibration	2 fs	1 million	2 ns
Production	2 fs	2.5 million	5 ns

2.2. Code optimisation

The analysis code from last semester's analyses was improved upon, and new optimisation techniques were introduced into the analysis code this semester, which enabled shorter run-times. Improvements were needed as the programs developed in first semester ran slowly on our home computers, necessitating access to university workstations to run multiple programs across different cores efficiently. However, throughout this semester our mobile workstation access was limited, and we had to rely on our personal computers. Slow run-times would have significantly hampered our progress, limiting the overall quantity of results produced and making the process of resolving errors in the analysis codes inefficient. Moreover, without optimisation the analysis of systems larger than that used would be prohibitively time consuming. Therefore, early on in this part of the project time was spent making basic efficiency improvements. Further gains in efficiency were achieved by switching some of our analyses programs from Python to Cython, a superset of the Python programming language with C-like performance [23]. This helped speed up the execution of our Python codes using fast C modules. Additionally, we changed our method for reading in large CSV data files, switching from `genfromtxt` to `pandas`. This in itself considerably reduced run-times, for example reducing a 23-minute run to a mere 32 seconds. This adjustment was highly valuable for re-running codes during testing. Previously only short snippets of data, such as CSVs with 10 steps, which had limited use as codes could only be tested over a very small number of timesteps.

One of the key strategies used was the removal of duplicate counting in the analysis codes by changing how the ij pairs were iterated over. Rather than iterating both i and j over all indicies, we changed the code to look at the oxygen atoms only (knowing their positions as the atoms are ordered in the data files as `C,C,...C,O,H,H,O,H,H,...`). The code that determined the iteration procedure was changed from

```
for i in range(0,N):
    if atom_type [i]==2:
        for j in range (0,N):
```

```
            if atom_type [j]==2 and i!=j:
```

to the following

```
for i in range (C, N - 5, 3):      #format: range (start, end, stepsize)
    for j in range (i + 3, N - 2, 3):
```

where `C` gives the position of the first `O` after all the `C`s in the data file and the 3 stepsize skips over the hydrogen atoms. Starting the j index from `i+3` reduces the number of counts by half, as ij and ji are no longer both counted. The end points `N-5` and `N-2` just give the last and second-to-last oxygen atoms. Also, bypassing the `atom_type` column from the file saves memory and time as the code does not keep checking for the right atom while still finding all the pairs needed. This resulted in a decrease of (approximately) 97% in the number of pair iterations, taking the $\rho = 1.0$ g/cm^3 system as an example, where approximately 23 million iterations (equal to N_{total}^2 where $N_{total} = 4815$ (see Table 1)) were reduced to 0.78 million ($(N_O^2)/2$ where $N_O = 1245$).

Table 3: The effect of optimisations on run-times for $\rho = 1.0$ g/cm^3 (* = estimated).

Code	Mass density	Dipole orientation	HB orientation	PDF_{OO}
Old	40 minutes	3.27 hours	-	17 hours
New	3.93 minutes	20.4 minutes	3.24 hours	6 hours*

2.3. Dipole orientation

The orientation of dipoles was analysed for the first layer at each density. The angle μ of the dipole $\hat{\mathbf{u}}$ is taken with respect to the direction normal to the interface, $\hat{\mathbf{z}}$ (Figure 3).

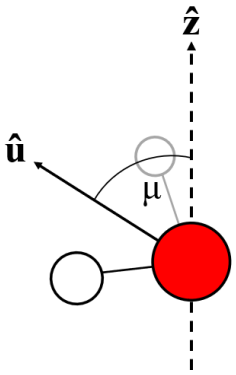

Figure 3: The definition of the dipole angle, μ.

2.4. Hydrogen bond orientation

The orientations of the water molecules was further analysed by examining the distribution of hydrogen bond directions. The hydrogen bond angle, θ_{HB}, was defined as the angle of the hydrogen bond with respect to the z-axis unit vector (perpendicular to the graphene surface), and is illustrated in Figure 4.

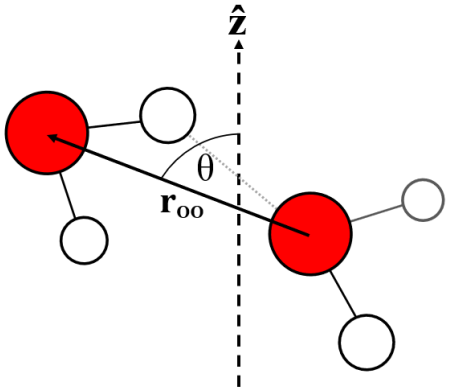

Figure 4: The definition of the hydrogen bond angle, θ_{HB}.

3. Results

3.1. Pair distribution functions

Figure 5 provides the g_{OH} and g_{HH} distribution functions (previous result for g_{OO} is provided in Figure 15 in the Appendix for comparison). The structure can be interpreted by comparing with the distribution of bulk water. Figure 5a shows peaks at 1.7Å, 2.4Å and 5.8Å, with a minima at 3.2Å. The position of the first peak remains unchanged compared with the bulk, as 1.7Å represents the nearest-neighbour peak (the surrounding atoms directly bonded with a given atom). Each subsequent peak represents the hydration shells: the shell(s) formed by the atoms bonded to the nearest neighbours and so on. The second peak shifts slightly closer, and the third further away, relative to the bulk. The 2.4Å peak represents the hydrogen bond, as this is the critical oxygen-hydrogen distance (for two atoms to be considered hydrogen bonded). Hence this value becoming shorter at higher densities corresponds to shorter hydrogen bonds being formed on average. It can also be seen that the hydrogen bond peaks become somewhat more pronounced at higher densities. This can be ascribed to the hydrogen bond network becoming more regular, shifting towards more solid-like behaviour. The above observations are similar to those found for g_{OO}, but here confirm that the oxygen-hydrogen bond itself is shortened. Data from Li *et al.* (2020) is plotted to illustrate that our results are consistent with the literature, though this result is for a 2.6 nm slit separation [24]. Mosaddeghi *et al.* (2012) also present similar results [25].

Figure 5b displays peaks at 2.4Å, 3.9Å and 6.2Å, with the first minima at 3.0Å. As before, the first peak only changes with intensity. The second peak becomes somewhat shorter at higher densities. We were unable to find hydrogen-hydrogen pair distribution functions in literature for the confined case. Liu *et al.* (2018) reported the first two peaks in g_{HH} at $r = \sim 2.4$Å and ~ 3.8Å for bulk water, which is consistent with our findings [26].

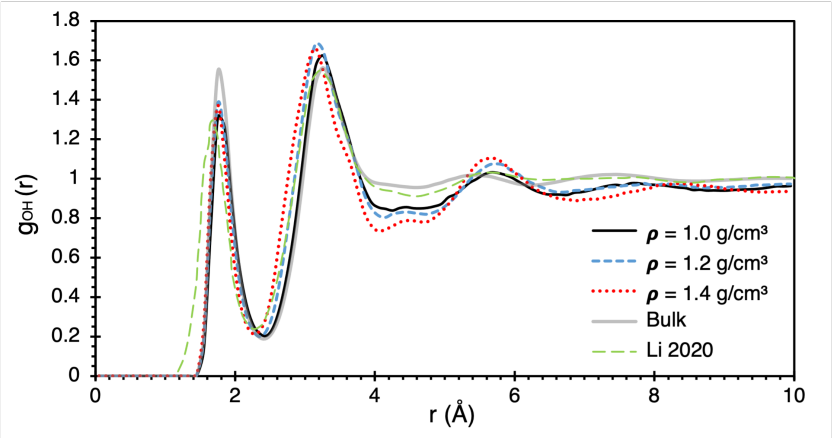

(a)

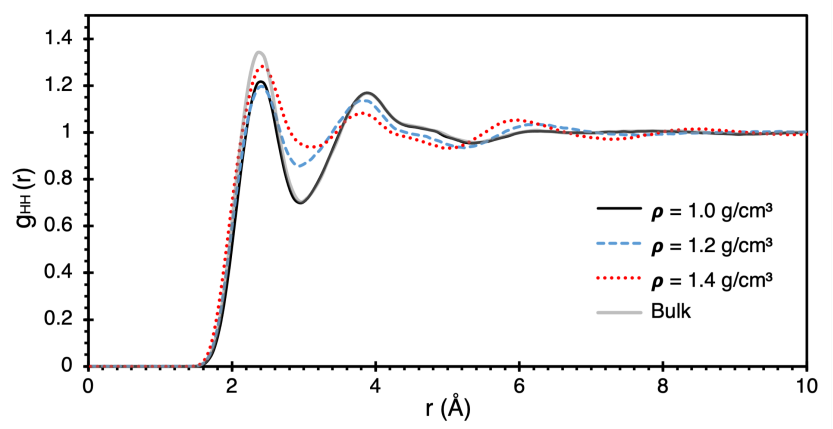

(b)

Figure 5: Partial distribution functions (PDFs) for the first layer of the system across densities. Plot (a) shows g_{OH}, the distribution for oxygen-hydrogen bonding, with a comparison to recent literature [24]; (b) shows g_{HH}, the distribution for hydrogen-hydrogen bonding. The bulk water results are plotted for reference.

3.2. Hydrogen bond number density

Figure 6 shows how the average number of hydrogen bonds per molecule varies with z. In the analysis, the program identified each hydrogen bond, labelled each oxygen atom based on how many hydrogen bonds it was associated with, then summed the number of oxygen atoms with each number of hydrogen bonds in a given volume slice before dividing by the total number of atoms in that slice.

This builds on the results found for the average number of hydrogen bonds per molecule in the previous semester, the results of which are illustrated in Figure 14 in the Appendix. The reduction in hydrogen bonds is linked to increased frequency of 2 and 3 bonds over 4 and 5 bonds. This effect is strongest closest to the confining wall, eventually becoming more bulk-like by the start of the second layer (for z greater than the first minima in the density distribution).

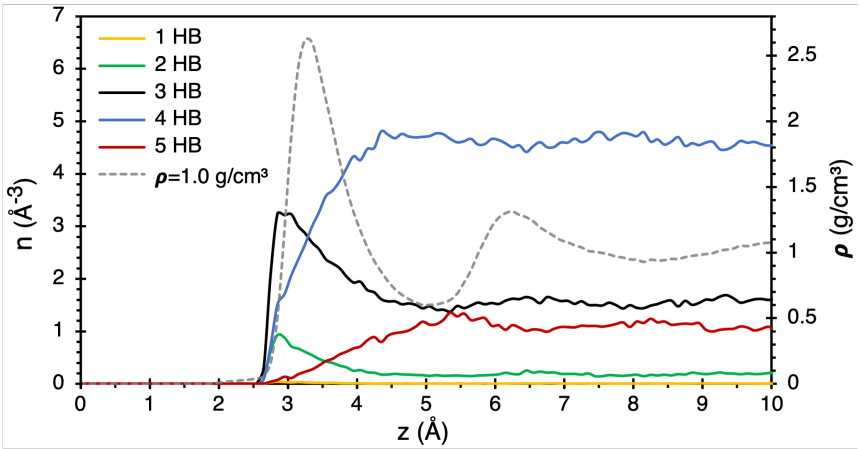

Figure 6: Frequency of molecules with a given number of hydrogen bonds as a function of the perpendicular distance from the confining wall, with the $\rho = 1.0$ g/cm^3 cross-sectional density distribution also plotted.

3.3. Dipole orientation

Figure 7 shows the relative probability distributions of $\cos(\mu)$ at different densities for the first layer. Figure 8 then illustrates how the distribution changes between layers for $\rho = 1.0$ g/cm^3. The two peaks, notable at higher densities, correspond to dangling bonds and hydrogen-bonding in-plane respectively. The comparisons made with the literature for this quantity demonstrate that the method used is bench-marked accurately. A polar representation of the relative probability distribution $P(\mu)$ is provided in Figure 9 which helps visualise clearly the preferential orientation of dipoles. Peak values were taken from the $\rho = 1.4$ g/cm^3 data, which has the most well-defined peaks. The first peak at $123.5° \pm 0.1°$ represents the dangling bond: an oxygen-hydrogen bond perpendicular to

the confining surface. We know this because the H-O-H angle in a given water molecule is 109.47°, this means that the angle between the O-H bond and the dipole vector is half this angle, 54.735°. It follows that 180° minus 54.735° equal to 125.3° is the predicted peak for dangling bonds. The second peak at $81.4° \pm 0.1°$ represents bonding in the plane parallel to the surface. The isotropic bulk distribution can be seen for $P(\mu) = 0.5$. The two emergent peaks become more clear with increasing density, though all densities show preferential orientation about 90°. Dipoles found near parallel (oriented 0° or 180° are assumed to be a result of thermal noise, and are reduced with increasing density. Other layers are not shown for clarity, but these were mostly bulk-like.

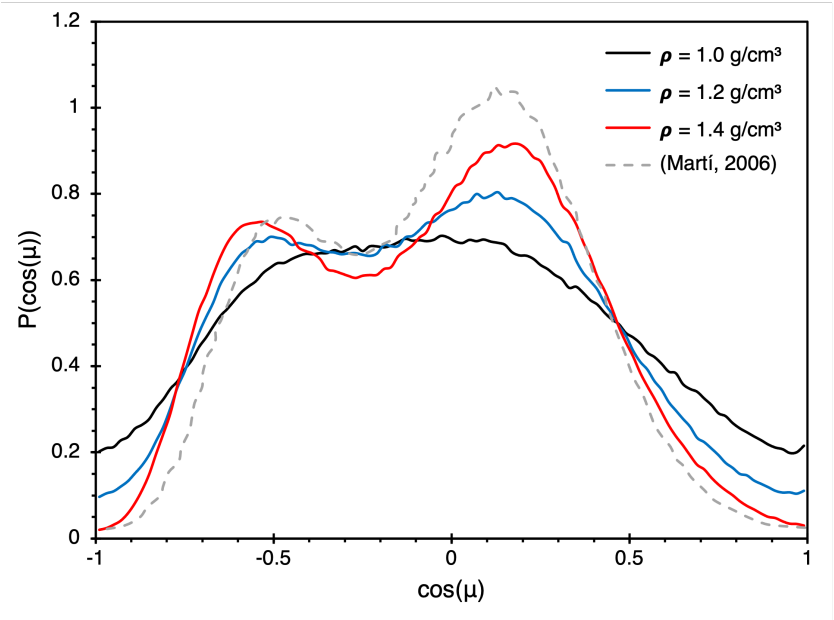

Figure 7: Distribution of $P(\cos(\mu))$ for the first layer at each density with literature comparison [13].

Our result for the preferential orientation of the water molecules is contrary to that claimed by Jalali *et al.* (2021), who assert that for a pure system of water molecules confined between graphene walls the preferred dipole orientation is perpendicular to the surface, along the z-axis and directed away from the surface [27]. Figure 10 shows how the orientation of the dipole varies along the cross section from the interface. This is helpful in showing the vertical distribution, however the averaging process somewhat

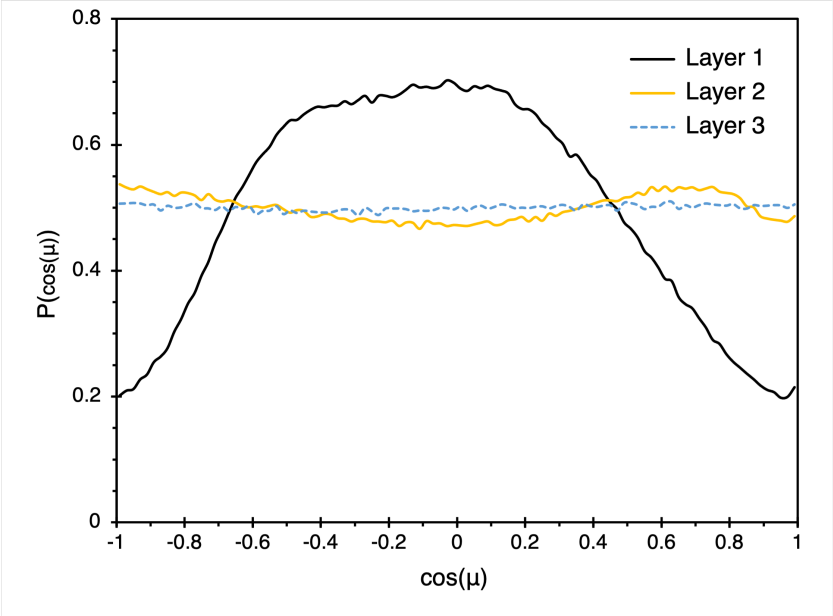

Figure 8: Distribution of $P(\cos\mu)$ for each layer at $\rho = 1.0$ g/cm^3.

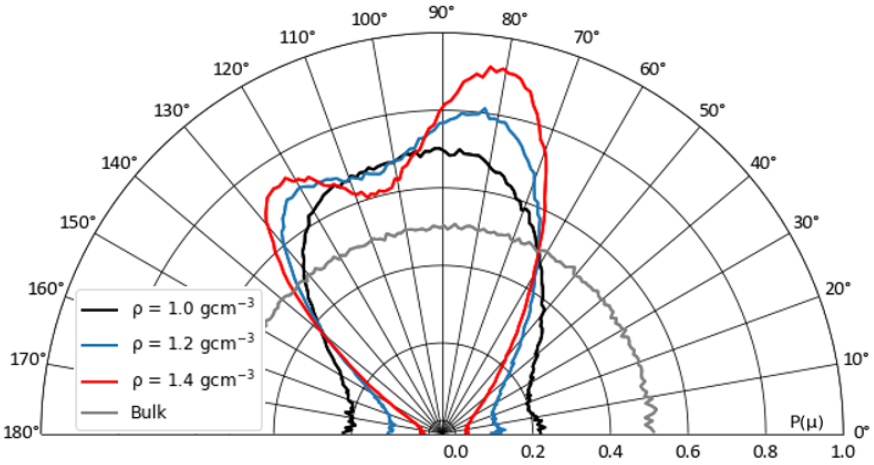

Figure 9: Polar plot of $P(\cos\mu)$ for the first layer at each density. Note that 0° corresponds to the $\hat{\mathbf{z}}$ direction perpendicular to the graphene sheet.

obscured the pattern as we averaged over positive and negative values.

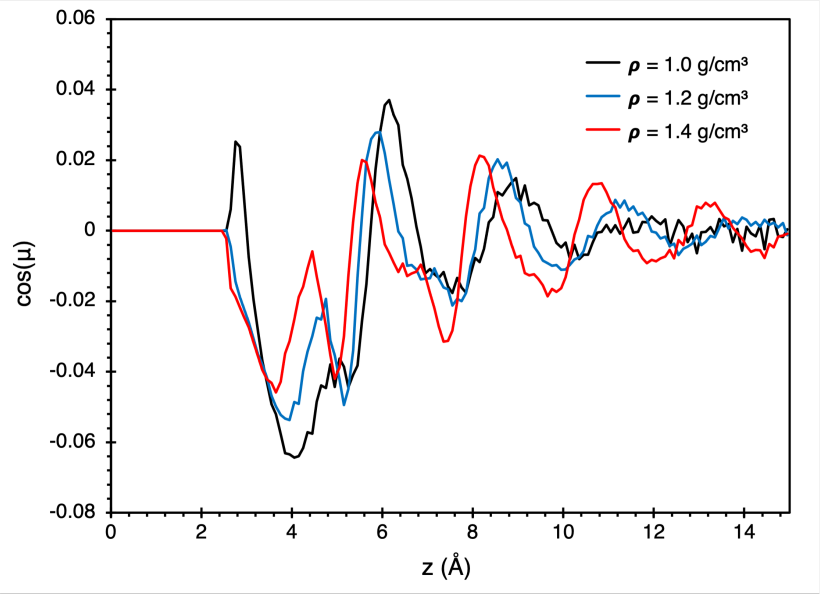

Figure 10: Distribution of average $\cos(\mu)$ as a function of z (distance from the graphene wall). Some information is lost in this representation, as we are averaging over positive and negative values. For example, for an average $\cos(\mu)$ value of zero, all you can interpret is that the distribution is symmetrical in some way.

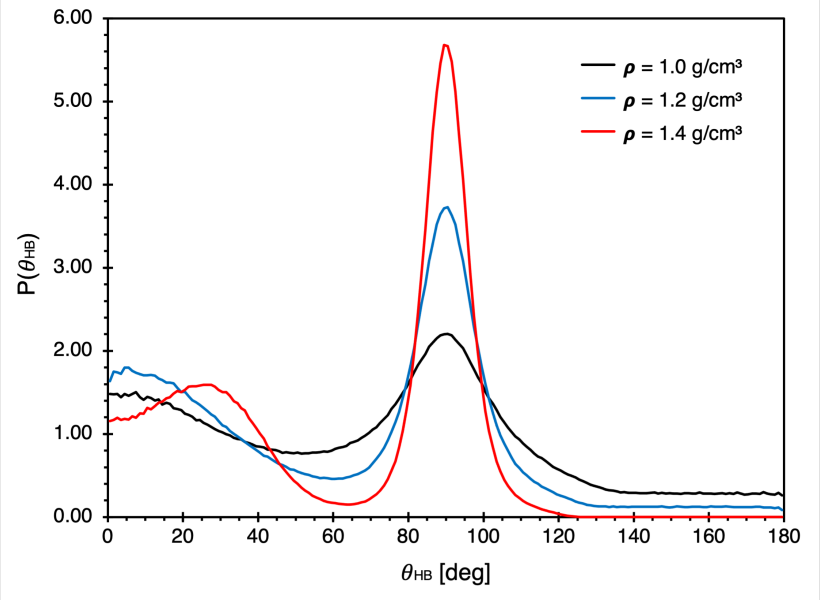

Figure 11: Distribution of $P(\theta_{\mathrm{HB}})$ for the first layer at each density.

3.4. Hydrogen bond orientation

The orientation of the water molecules was characterised using a relative probability distribution $P(\theta_{\mathrm{HB}})$ of angles θ_{HB} between the hydrogen bond vectors and z-vector (normal to the graphene wall). Figure 11 shows $P(\theta_{\mathrm{HB}})$ for the different densities, while Figure 12 illustrates the structure between layers at each density separately. The distributions were normalised using the bulk values measured last semester. While no literature was found that provided a direct comparison with our representation, results from Ruiz-Barragan *et al.* (2019) offer a useful qualitative comparison [28]. Our findings confirm preferential planar hydrogen bonding in the interfacial later, while also showing the inter-layer bond structure.

4. Conclusion

The results of our MD simulations on water confined in a graphene slit have been presented for three different densities. The structural characteristics of water confined between two parallel graphene walls with periodic boundaries in-plane were studied using the SPC/E force field for interactions between water molecules, with Lennard-Jones parameters at the oxygen atoms which determined the water-carbon interaction. Our analyses of the water molecule orientation, including the orientation of dipoles and hydrogen bonding, have built upon work carried out in the previous semester. We successfully benchmarked a number of programs with literature, achieving results consistent with the theory that hydrogen bonding in confined water is restricted or suppressed. The orientational distribution of hydrogen bond vectors tells us that there is preferential bonding in the plane, with additional dangling-bond phenomena where a portion of hydrogen bonds are directed toward the confining surface. The radial pair distribution functions also show regularity, with highly structured distributions particularly at higher densities.

Nevertheless, our work is not sufficient to explain the full effects that produce such a low value of the dielectric constant as investigated experimentally by Fumagalli *et al.*

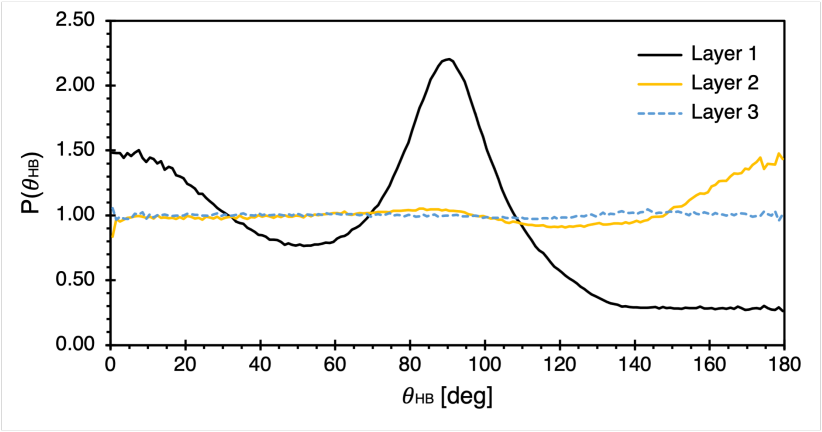

(a)

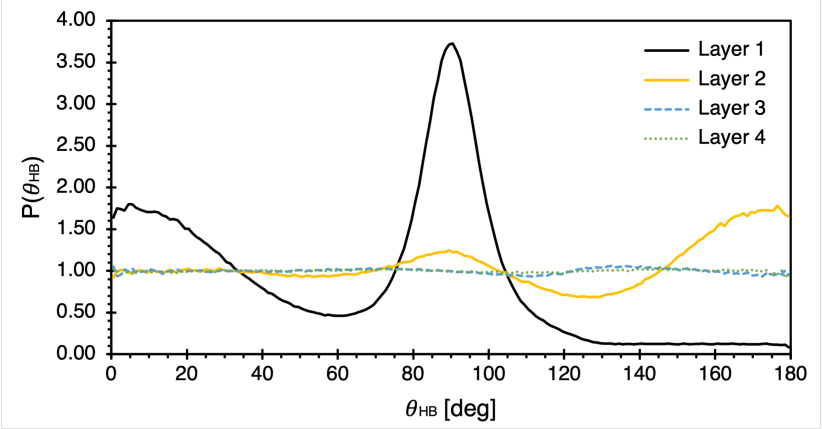

(b)

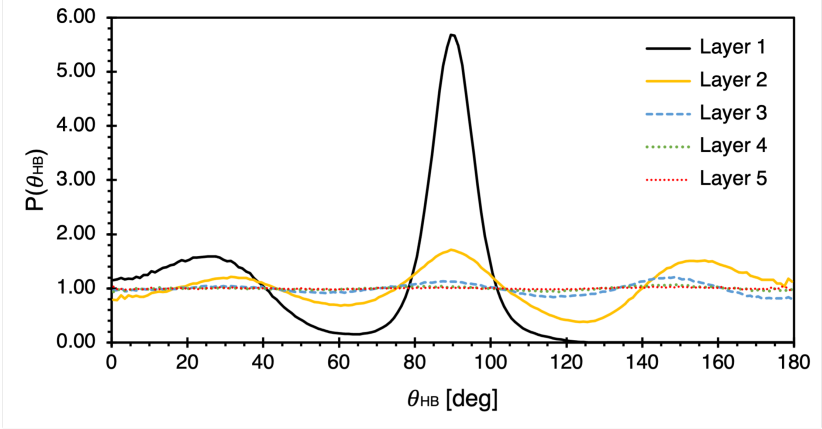

(c)

Figure 12: Distributions of $P(\theta_{\mathrm{HB}})$ for different layers at all three densities: (a) $\rho = 1.0$ g/cm^3, (b) $\rho = 1.2$ g/cm^3, (c) $\rho = 1.4$ g/cm^3.

(2018) [5]. Further work could be carried out to actually calculate the dielectric constant in our system. Despite this, our efforts to improve the analyses code this semester was useful and important. We did not have access to the workstation, so to produce the quantity of results we did it was necessary to make improvements and optimisations to the code. This allowed us to amend errors in the analysis much faster than we would otherwise have been able to.

Overall, we succeeded in our main objectives for this project. We learnt how to run molecular dynamics simulations, including the main concepts in MD simulation and software, and wrote a number of programs to analyse obtained trajectories of simulated water and applied these to the case of confined water. In review, utilising the O-H angle instead of the hydrogen bond angle in our analysis may have proved more useful, as there are more results in the literature for the O-H angle definition. This work could be extended by analysing simulations over a range of slit separations. Additionally, temperature effects could be investigated. Furthermore, the nature of the confining surface could be explored, by studying a range of hydrophobic materials to identify common trends across these, or using hydrophilic surfaces to compare differences between the two.

References

[1] C.-Y. Lee, J. A. McCammon, and P. J. Rossky, "The structure of liquid water at an extended hydrophobic surface," *The Journal of Chemical Physics*, vol. 80, no. 9, pp. 4448–4455, 1984.

[2] K. S. Novoselov, A. K. Geim, S. V. Morozov, D. Jiang, Y. Zhang, S. V. Dubonos, I. V. Grigorieva, and A. A. Firsov, "Electric field effect in atomically thin carbon films," *Science*, vol. 306, no. 5696, pp. 666–669, 2004.

[3] K. S. Novoselov, D. Jiang, F. Schedin, T. J. Booth, V. V. Khotkevich, S. V. Morozov, and A. K. Geim, "Two-dimensional atomic crystals," *Proceedings of the National Academy of Sciences*, vol. 102, no. 30, pp. 10451–10453, 2005.

[4] M. C. Gordillo and J. Martí, "Structure of water adsorbed on a single graphene sheet," *Physical Review B*, vol. 78, no. 7, 2008.

[5] L. Fumagalli, A. Esfandiar, R. Fabregas, S. Hu, P. Ares, A. Janardanan, Q. Yang, B. Radha, T. Taniguchi, K. Watanabe, G. Gomila, K. S. Novoselov, and A. K. Geim, "Anomalously low dielectric constant of confined water," *Science*, vol. 360, no. 6395, pp. 1339–1342, 2018.

[6] B. Halle, *Hydration Processes in Biology*, p. 233. Ohmsha: IOS Press, 1999.

[7] D. Chandler, "Interfaces and the driving force of hydrophobic assembly," *Nature*, vol. 437, pp. 640–647, 2005.

[8] W. Kauzmann, "Some factors in the interpretation of protein denaturation," *Advances in Protein Chemistry*, vol. 14, pp. 1–63, 1959.

[9] N. Eliaz and E. Gileadi, *Physical Electrochemistry: Fundamentals, Techniques, and Applications*. Wiley, 2019.

[10] J. Li, T. Liu, X. Li, L. Ye, H. Chen, H. Fang, Z. Wu, and R. Zhou, "Hydration and dewetting near graphite-CH3and graphite-COOH plates," *The Journal of Physical Chemistry B*, vol. 109, no. 28, pp. 13639–13648, 2005.

[11] D. Frenkel and B. Smit, *Understanding molecular simulation*. No. 1 in Computational science series, San Diego, California: Acad. Press/Elsevier, second ed., 2002.

[12] G. Cicero, J. C. Grossman, E. Schwegler, F. Gygi, and G. Galli, "Water confined in nanotubes and between graphene sheets: a first principle study," *Journal of the American Chemical Society*, vol. 130, no. 6, pp. 1871–1878, 2008.

[13] J. Marti, G. Nagy, M. C. Gordillo, and E. Guàrdia, "Molecular simulation of liquid water confined inside graphite channels: Thermodynamics and structural properties," *The Journal of Chemical Physics*, vol. 124, no. 9, p. 094703, 2006.

[14] S. Plimpton, "Fast parallel algorithms for short-range molecular dynamics," *Journal of Computational Physics*, vol. 117, pp. 1–19, 1995. http://lammps.sandia.gov.

[15] L. Martínez, R. Andrade, E. G. Birgin, and J. M. Martínez, "Packmol: A package for building initial configurations for molecular dynamics simulations," *Journal of Computational Chemistry*, vol. 30, no. 13, pp. 2157–2164, 2009.

[16] Agilio Padua, "fftool v1.0.0," 2015. This is a Python tool to build force field input files for molecular dynamics simulations of systems composed of molecules, ions or extended materials.

[17] M. Born and T. von Karmann, "Über Schwingungen in Raumgittern," *Physik. Z.*, vol. 13, pp. 297–309, 1912.

[18] H. J. C. Berendsen, J. R. Grigera, and T. P. Straatsma, "The missing term in effective pair potentials," *The Journal of Physical Chemistry*, vol. 91, no. 24, pp. 6269–6271, 1987.

[19] A. Y. Toukmaji and J. A. Board, "Ewald summation techniques in perspective: a survey," *Computer Physics Communications*, vol. 95, no. 2-3, pp. 73–92, 1996.

[20] M. P. Allen, *Computer simulation of liquids*. Oxford: Oxford University Press, second edition ed., 2017.

[21] W. Humphrey, A. Dalke, and K. Schulten, "VMD – Visual Molecular Dynamics," *Journal of Molecular Graphics*, vol. 14, pp. 33–38, 1996. http://www.ks.uiuc.edu/Research/vmd/.

[22] D. C. Rapaport, *The art of molecular dynamics simulation*. Cambridge: Cambridge University Press, second edition ed., 2004.

[23] S. Behnel, R. Bradshaw, C. Citro, L. Dalcin, D. S. Seljebotn, and K. Smith, "Cython: The best of both worlds," *Computing in Science & Engineering*, vol. 13, no. 2, pp. 31–39, 2011.

[24] F. Li, I. A. Korotkin, and S. A. Karabasov, "Rheology of water flows confined between multilayer graphene walls," *Langmuir*, vol. 36, no. 20, pp. 5633–5646, 2020.

[25] H. Mosaddeghi, S. Alavi, M. H. Kowsari, and B. Najafi, "Simulations of structural and dynamic anisotropy in nano-confined water between parallel graphite plates," *The Journal of Chemical Physics*, vol. 137, no. 18, p. 184703, 2012.

[26] J. Liu, X. He, J. Zhang, and L.-W. Qi, "Hydrogen-bond structure dynamics in bulk water: insights from ab initio simulations with coupled cluster theory," *Chemical Science*, vol. 9, no. 8, pp. 2065–2073, 2018.

[27] H. Jalali, E. Lotfi, R. Boya, and M. Neek-Amal, "Abnormal dielectric constant of nanoconfined water between graphene layers in the presence of salt," *The Journal of Physical Chemistry B*, vol. 125, no. 6, pp. 1604–1610, 2021.

[28] S. Ruiz-Barragan, D. Muñoz-Santiburcio, and D. Marx, "Nanoconfined water within graphene slit pores adopts distinct confinement-dependent regimes," *The Journal of Physical Chemistry Letters*, vol. 10, pp. 329–334, 2019.

A. Previous results

Key plots for the structural properties of the confined water system produced last semester are presented here. These include plots of mass density distribution (Figure 13), average number of hydrogen bonds per molecule (Figure 14), and oxygen-oxygen pair distribution functions (Figures 15 and 16). The latter can be compared with g_{OH} and g_{HH} distributions in Section 3.1. Note the legends: blue and red are inverse of the colour scheme used throughout this report.

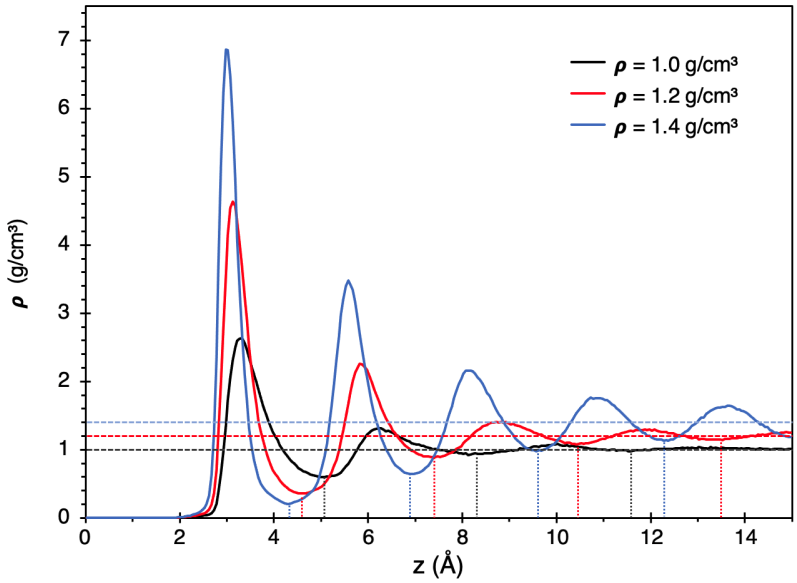

Figure 13: Mass density distributions of confined water for each density simulated. The horizontal dashed lines represent the bulk densities, and illustrate how the layered distribution of the interfacial water converges to the bulk (becomes more 'bulk-like') in the innermost layer between the grahite sheets. The vertical dashed lines mark the minima of the confined system density distributions. These were used to define the different layers.

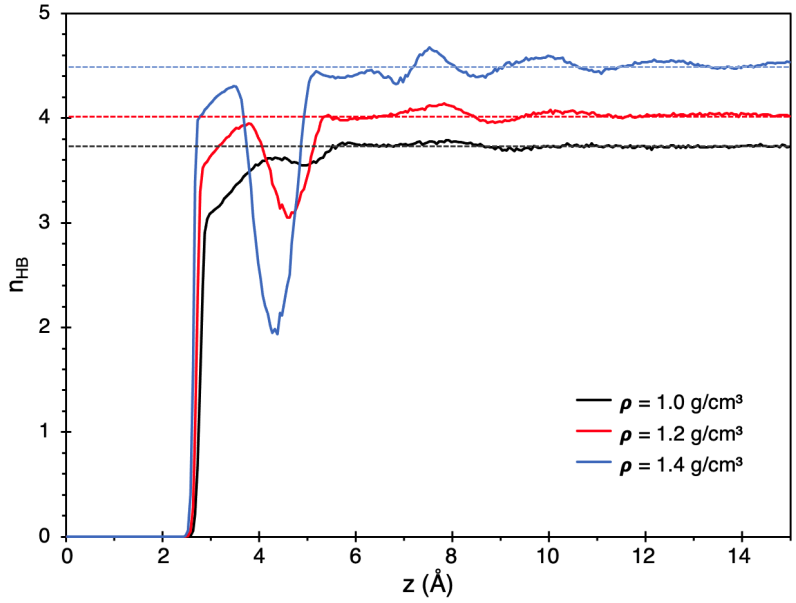

Figure 14: Hydrogen bonds per molecule as a function of z for each density. The horizontal dashed lines represent the number of hydrogen bonds per molecule for bulk water. The confined systems converge to the bulk values in the inner region of the slit.

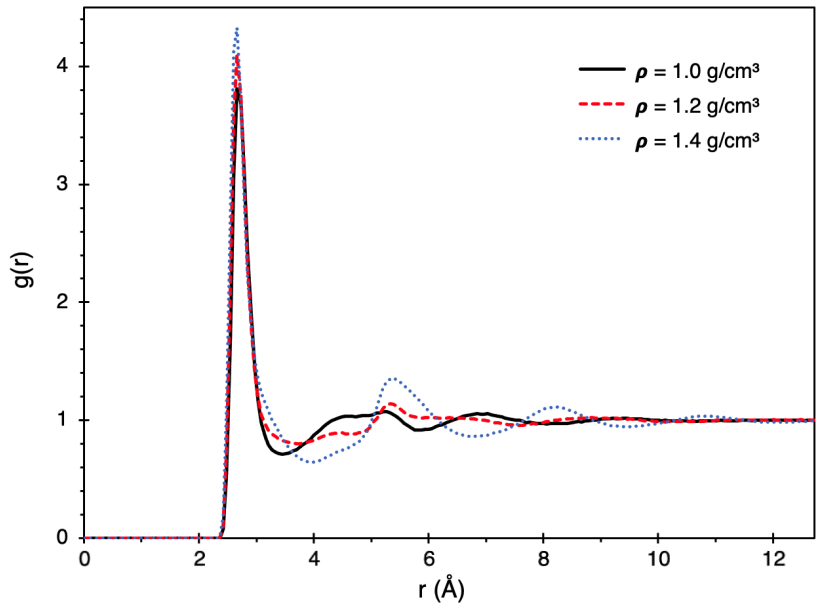

Figure 15: Oxygen-oxygen pair distribution functions for the first (interfacial) layer at each density.

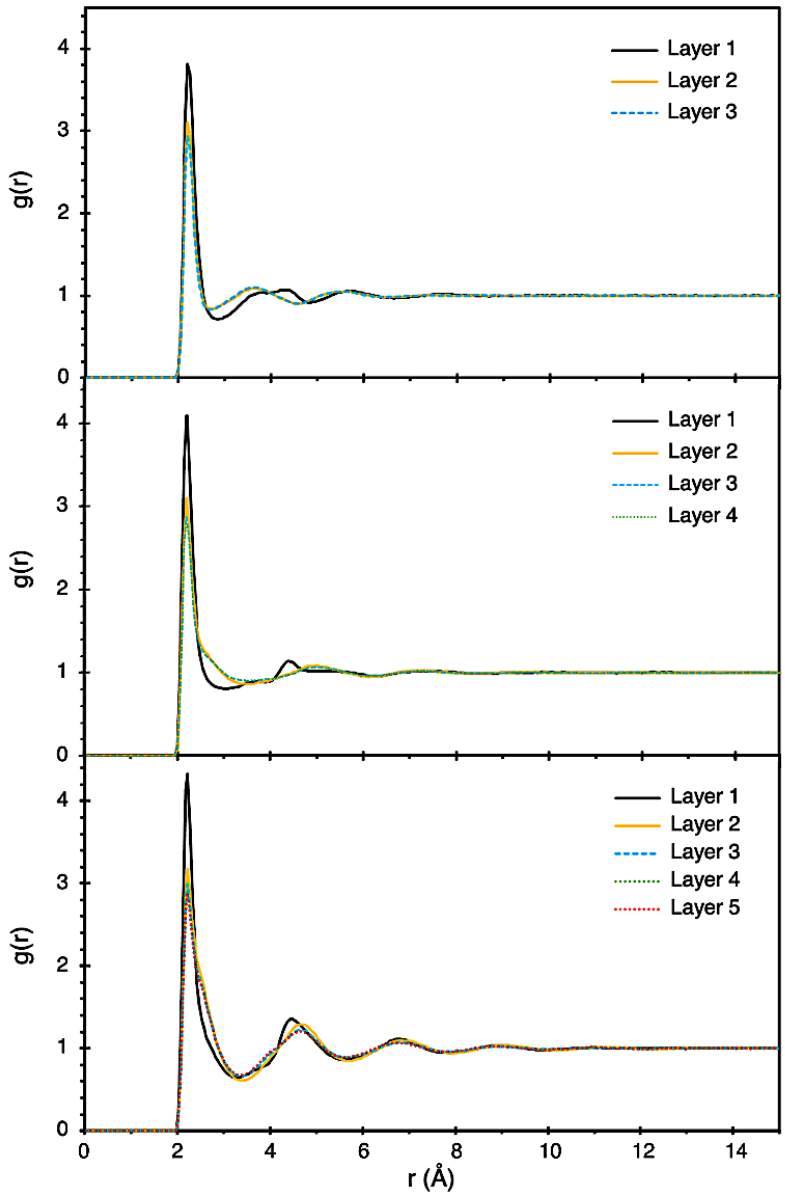

Figure 16: Oxygen-oxygen pair distribution functions for different layers at each density, $\rho = 1.0, 1.2, 1.4$ g/cm^3 from top to bottom. Subsequent minima in the density profile (Fig.13) define each layer. Note the error: these plots were accidentally shifted approximately 0.5Å to the left.